EXPERIMENTAL INVESTIGATION ON PROPELLER SLIPSTREAM INTERFERENCE EFFECTS ON A SWEPT WING AT LOW SPEED CONDITIONS

by

J. Prijo Kusumo Aero-Gasdynamics and Vibration Laboratory (LAGG - BPPT)
N. Gayus P.T. Industri Pesawat Terbang Nusantara (IPTN)
L.G.M. Custers National Aerospace Laboratory (NLR)
L.H. de Haij Fokker Aircraft B.V.
L.L.M. Veldhuis Delft University of Technology

Abstract

A half-span swept wing model was used to investigate propeller slipstream effects within a joint research program between IPTN, LAGG, ITB, Fokker Aircraft B.V, NLR and TU Delft.The test was performed in the 3 by 4 meters Indonesian Low Speed Wind Tunnel (ILST) LAGG in Serpong Indonesia. The aim of the program was to investigate the propeller / wing / flap interaction on a typical transonic wing design at low speed conditions. The model consisted of 5 main components ; Wing, Flap, Nacelle, Propeller and Fuselage. In the prop-on case the model was powered by a 1/5 scale model of the Fokker 50 6-bladed propeller. Force and moment data were obtained by means of the combination of both an external balance and a rotating shaft balance (RSB), both of which capable of measuring 6 components. The wing and flap were equipped with respectively 9 and 5 pressure stations.

The simultaneous use of a rotating shaft balance and an external balance enabled the determination of the slipstream interaction forces between propeller and the wing. During the measurements the thrust of the propeller could be controlled by means of the RSB. By knowing directly the thrust applied on the shaft combined with the axial force measured by the external balance, the drag acting on the wing / nacelle / flap combination could be determined on-line. Pressure measurements on the wing and flap showed the influence of the propeller slipstream on the sectional pressure distribution and the spanwise lift distribution.

The test results discussed in this paper are based on a test condition with a thrust coefficient of 2.5 and a 15 degree flap angle setting.

Nomenclature

b/2	semi span of the half model	(m)
c	chord	(m)
$\bar{c}$	mean aerodyamic chord	(m)
c_l	local lift coefficient $= c_N \cos\alpha - c_T \sin\alpha$	
C_D	drag coefficient = D /q S_w	
C_L	lift coefficient = L /q S_w	
c_N	local normal force coefficient $= -\frac{c}{\bar{c}} \oint c_p d\frac{x}{c}$	
c_p	pressure coefficient $= \frac{p_i - p}{q_\infty}$	
c_T	local axial force coefficient $= +\frac{c}{\bar{c}} \oint c_p d\frac{z}{c}$	
D	drag, diameter	(N)
J	advance ratio = V /N Dp	
L	lift force	(N)
l	local lift	(N/m)
N	rotational speed	(rps)
p	pressure	(Pa)
q	dynamic pressure	(N/m^2)
S	area	(m^2)
T	propeller thrust	(N)
T_c	thrust coefficient = propeller axial thrust/q S_p	
V	tunnel velocity	(m/s)
y/(b/2)	spanwise position	
x/c	orifice position in axial direction	
z/c	orifice position in normal direction	

subscripts

ax	axial
b	body
f_a	free air
i_{nst}	installed
i_{so}	isolated
j	jet
n	nacelle
p	propeller, propulsive
s	slipstream
sh	shaft
w	wing
wn	wing+nacelle (in the blades-on configuration)
wnp	wing+nacelle+propeller
wn0	wing+nacelle (in the blades-off configuration)

Introduction

Interference effects on a wing/flap combination and the propeller installation are especially important at low speed conditions like the second segment-climb with one-engine inoperative and landing approach conditions. The effect of increased wing-upwash due to flap extension and the effect of wing sweep will affect the propeller force characteristics.

In a joint Indonesian/Dutch effort by IPTN, LAGG, ITB, Fokker, NLR and the Technical University of Delft an experimental investigation was performed to provide insight into the magnitude of the above mentioned effects on a typical transonic configuration at low speed condition (wingsweep, flaps extended).

The paper briefly described the test set-up in the 3 by 4 meters Indonesian Low Speed Wind Tunnel (ILST) using a half model with a 2.1 m half span on which a 0.70 m diameter propeller was mounted. To study the interaction effects with higher lift coefficients a flap could be mounted, covering about 80% of the span. Wing, flap and fuselage were all extensively equipped with pressure taps.

Examples of the test results are used to illustrate the benefits of the use of both a rotating shaft balance and an external balance which provides the opportunity to determine the interaction forces on both propeller and wing, as well as the propeller thrust during the measurements. The combination of the pressure measurements and the forces measurements has produced a valuable data base for study of the various interference effects, which is briefly discussed.

Test set-up

Test Facility

The test was performed in the ILST, an atmospheric closed -circuit windtunnel. It has a closed test section with a rectangular cross section of 4 m wide and 3 m high and a length of 8.75 m. The ILST has been designed to have air speed range between 0 - 110 m/s in empty tunnel condition. A lay-out of the ILST is shown in figure 1.

A six component external balance measures forces and moments of the model mounted on the test section. The ILST is also equipped with a compressed air system which supplies the high pressure drive air to the model. This system has a sustained maximum air flow rate of 6 kg/s and a maximum pressure of 100 bar. The system includes a sonic venturi for accurate mass flow determination. The total pressure downstream of the venturi is measured to verify its choked condition. The mass flow is controlled upstream of the critical venturi by a mass flow control station. Maximum mass flow during the test was 0.88 kg/s at upstream venturi total pressure of 55 bar.

Model interface

The model described in the next chapter was installed on an interface mounted to the six-component external balance. The model can be rotated about the external balance y-axis to provide angle of attack variation.

The air supply is led across the external balance to the strut by means of a low reaction air bridge. This ensures minimal interference effects of the air flow on the external balance which could be corrected for.

In order to minimize boundary layer effects due to tunnel wall, a boundary layer plate (Peniche) was mounted as interface between tunnel wall and model. A labyrinth seal between the peniche and the model was used to minimize flow leakage from the downside to the topside of the model. To monitor if touching occured in the labyrinth, an electric fouling device was used during the execution of the test. Also some pressure taps were installed in the labyrinth to monitor the static pressure distribution along the peniche.

Model description

A half-span starboard wing model without a tailplane was used for the test in the ILST. The main structural parts of the half model consisted of the Fuselage, Wing, Flap, Nacelle and Propeller. Figure 2 shows the model installed in the test section. The model was designed by Fokker Aircraft B.V. and was manufactured by both LAGG and IPTN, with support from NLR in the stuctural design. The general arrangement of the half model is shown in figure 3 which consists of three views : upper -, front - and side view with the model dimensions. The figure also shows the basic configurations of the model.

The model has a fuselage body designed to simulate a high-wing configuration. The fuselage was mounted to the external balance with an off-set from the tunnel wall in order to reduce wall boundary layer effects, as discussed above. The fuselage was also equipped with a number of pressure orifices divided into three stations in streamwise direction in order to evaluate pressure distribution over the fuselage body.

The wing is a typical transonic wing with a half-span of 2.1 m and equipped with nine pressure stations each with 25 pressure orifices. The air feed and the instrumentation cabling for the air motor, and the pressure tubing for the pressure stations are completely buried inside the wing. In order to fix the transition position over the wing a tripping strip with 0.25 mm thickness was placed along the wing span at 10 % local chord on the upper surface and 30 % on the lower surface.

The model was fitted with a single slotted flap equipped with 5 pressure stations each with 12 pressure orifices. The ratio of flap chord to wing chord is 32 % and the flap extends to about 80 % wing span. The flap deflection angle was 15 degrees.

The nacelle is a slender body of revolution, housing the TDI 1555A turbine air motor, a 5 to 1 reduction gearbox and a turbine exhaust duct. The exhaust shape is a standard ASME nozzle and is equipped with total temperature and total pressure rake, placed just ahead of the nozzle. For the simulation of natural blowing and during exhaust calibrations, the air turbine motor was replaced by a throttle plate.

The 4-component rotating shaft balance (RSB) is placed between the drive shaft and the propeller hub. NLR designed this balance suitable for a maximum load of 1250 N (axial force) and 125 Nm (torque), and 600 N and 40 Nm for respectively the off-axis force and moment. The off-axis force and moment can be decomposed by using a 24-channel 16-bit FFT system into normal force, side force, yawing moment, and pitching moment. To decompose the forces and moments a magnetic sensor was incorporated in the air turbine motor and was used as an azimuth maker. As shown in figure 4 the inner ring mounted on the drive shaft is the non-metric part while the hub and the propeller are mounted on the metric outer ring.

The model propeller used during the test is a 1:5 scaled version of the 6-bladed Fokker 50 propeller and has a diameter of 0.73 m. The direction of the propeller rotation is clockwise as seen in the direction of flight. The propeller blades were mounted in an alumunium hub. In order to be able to account for the pressure term acting on the aftside of the hub, a 'backplate' was added to the rotating hub. A plate equipped with 36 pressure taps placed in an area-weighted pattern, was mounted opposite of the backplate onto the nacelle.

Data Reduction

Data Acquisition

A scheme of the data acquisition and data processing system is shown in figure 5. For the test a Fast Fourier Transform (FFT) system has been used in order to support the determination of the off-axis components of the forces and moments measured by RSB.

Basically all the recorded data were treated as stationary signals, except for the unsteady cyclic (instationary) signals from the RSB off-axis components of the forces and moments. The acquisition of these signals was controlled by the data acquisition system. The instationary signals were amplified by the signal conditioning units and subsequently led to the FFT-system. A trigger pulse generated by the air turbine motor was used by the FFT-system to trigger data sampling and to permit recording of the RSB azimuthal position.

Communication between the FFT-sytem and the data processing sytem was realized by use of the local area network. The results of the FFT-system were used in the APROPOS on-line data processing.

Data Processing

Several model configurations were tested to determine model tare lift and drag, jet thrust, spinner tare force and propeller thrust, see figure 3. Forces and moments were measured using both the external balance and the RSB.

The origin of all external balance data is the model reference point (MRP), located at 25 % MAC, see figure 6.

Using the results of the measurements on different model configurations and the combined use of a RSB and an external balance, it is possible to study the aerodynamic characteristics of the individual components, their mutual interference, and the overall aerodynamic characteristics. Because the bookkeeping is applied to a half model, the discussion is limited to lift and drag. In the discussion *lift* relates to all aerodynamic forces in the lift direction (perpendicular to the tunnel flow), including the contribution from propeller. The *drag* relates to all aerodynamic forces in streamwise (drag) direction, excluding the streamwise components of the propeller and jet thrust forces. Tables 1 and 2 provide an overview of the applied bookkeeping scheme for the configuration without flap.

The results of the pressure measurements are presented as pressure coefficients. To obtain the local section normal force- and axial force-coefficients, the pressure at each pressure station were integrated and normalized with the mean aerodynamic chord.

Table 1. Lift bookkeeping scheme

	Measured by the external balance				measured by the RSB	
Configuration	W	WN0	WN_{JET}	WNP	P_{inst}	P_{iso}
generates :	L_w	$L_{wn0}=L_w+\Delta L_n$	$L_{wnj}=L_w++\Delta L_n+\Delta L_j$	$L_{wnp}=L_w+\Delta L_n+\Delta L_j+\Delta L_p+\Delta L_s$	$L_p=L_{p0}+\Delta L_p$	L_{p0}
Minus result of :						
W		ΔL_n	$\Delta L_n+\Delta L_j$	$\Delta L_n+\Delta L_j+\Delta L_p+\Delta L_s$		
WN0			ΔL_j	$\Delta L_j+\Delta L_p+\Delta L_s$		
WN_{jet}				$\Delta L_p+\Delta L_s$		
WNP						
P_{inst}				$L_{wn}=L_w++\Delta L_n+\Delta L_j+\Delta L_s$		
P_{iso}					ΔL_p	
$WN0+P_{inst}$				$\Delta L_j+\Delta L_s$		
$WN_{JET}+P_{inst}$				ΔL_s		

Table 2. Thrust and drag bookkeeping scheme

	Measured by the external balance				measured by the RSB	
Configuration	WF	WN0	WN_{JET}	WNP	P_{inst}	P_{iso}
generates :	D_w	$D_{wn0}=D_w+\Delta D_n$	$T_j-D_{wnj}=T_j-D_w+\Delta D_n+\Delta D_j$	$T_{sh}+T_j-D_{wnp}=T_{sh}+T_j-(D_w+\Delta D_n+\Delta D_j+\Delta D_p+\Delta D_s)$	$T_p=T_{sh0}+\Delta T_{sh}$	$T_{stat}=T_{fs}+\Delta T_h$
Minus result of:						
WN0			ΔD_j	$T_p=T_{sh}-(\Delta D_j+\Delta D_p+\Delta D_s)$		
WN_{jet}				$T_p=T_{sh}-(\Delta D_p+\Delta D_s)$		
P_{inst}				$D_{wn}=D_w+\Delta D_n+\Delta D_j+\Delta D_s$		
P_{iso}					ΔT_{sh}	
$WN0+P_{inst}$				$\Delta D_s+\Delta D_j$		
$WN_{JET}+P_{inst}$				ΔD_s		

Test description

Tests were conducted on four main configurations ; Wing (W), Wing + Flap (WF), Wing + Nacelle (WN), and Wing + Nacelle + Flap (WNF). The prop-on test was performed for WN and WNF configurations (respectively referred to as WNP and WNFP). The prop-off test measurements were divided in two series. First the test with blowing nozzle (WNjet and WNFjet), followed by the test with faired nozzle (WN0 and WNF0). The blade pitch angle was set at 28^0 at 70% propeller radius. For the model configurations with the flap installed (WF and WNF), the flap angle setting was 15^0 . Both force and pressure data were taken simultaneously at angle of attack sweeps (ranging from -4^0 to 11^0) at constant tunnel velocity (40, 70 and 80 m/s), and constant thrust coefficient or nozzle pressure ratio (in the case of the blowing nozzle configuration).

The test results of the pressure measurements on both the flap-on and flap-off configurations are used in the discussion of the interference effects. The discussion of the force data is limited to the flap-off configurations. Comparisons between the propeller-on and propeller-off results are made for a thrust coefficient of 2.5.

Results and discussion

Pressure measurement

When a propeller produces thrust, the axial velocity behind the propeller increases and the tangetial velocity component in the slipstream produces a swirling flow. The altered flow field results in different sectional pressure distributions on the wing and the flap. These differences can be observed in the test results of the pressure distributions at the pressure stations directly inboard and outboard of the nacelle. These pressure stations are located within the slipstream of the propeller.

For the wing/nacelle-configuration, the comparison of the different pressure distributions with and without propeller is shown in figure 7 for the inboard wing section and in figure 8 for the outboard wing section. The upwash at the inboard section increases the local angle of attack, resulting in a very large suction peak and an increase of the local lift coefficient. The increased dynamic pressure in the slipstream is indicated by the increase of the positive pressure peak on the lower wing surface. On the outboard section the negative local angle of attack due to the propeller swirl results in a suction peak on the lower surface and a stagnation point on the upper surface. The large lift loss compared to the blades-off condition is clearly visible.

For the wing/nacelle/flap configuration the pressure distribution with and without propeller at about 5^0 angle-of-attack is shown in figures 9 and 10, respectively for the in- and outboard sections near the nacelle. The flap increases the suction peak at the wing nose relative to the flap-off configuration. Again the slipstream effects result in a large lift increase on the inboard wing section (figure 9) and a lift loss on the outboard wing section (figure 10). The dynamic pressure increase leads to a large load increase on the flap, for both the in- and outboard flap section. This indicates that the dynamic pressure increase in the slipstream is the main cause of the changes in the flap pressure distribution due to the propeller slipstream.

A comparison of the blades-on versus blades-off spanwise lift distribution is given for respectively the flap-on and flap-off configurations in figures 11 and 12. The airframe parts immersed in the slipstream are subjected to increased velocities and to the local variations in angle-of-attack, due to the swirl in the propeller slipstream. Directly outboard of the nacelle the local inflow angle are reduced, resulting in lower lift coefficients. Also the inboard parts not immersed in the propeller slipstream are apparently subject to a larger velocity. The combination of large velocities in the slipstream and the presence of a "gulley" between the nacelle and fuselage creates a local increase in velocity, resulting in a higher local lift. The large lift increase on the inboard parts of the wing more than offsets the lift loss on the parts directly outboard of the nacelle. The outboard parts of the wing which are not immersed in the slipstream, are hardly affected by the presence of the propeller. For the flap-on configuration a slight difference is visible which may be attributed to the slightly larger angle-of-attack.

For the flap-on configuration the local lift coefficient on the section directly outboard of the nacelle is still larger in the propeller-on condition. The lift increase of the flap more than offsets the lift loss of the wing section, see figure 10 and 11. Apparently the presence of the flap increases the gains in lift on the parts of the wing behind the up-going side of the propeller, and

also eliminates the lift losses on the parts behind the down-going side of the propeller.

Force measurement

Lift

By comparing the results of the configuration with propeller (WNP) and the configuration without propeller (WN0), the interference effects on the aerodynamic forces can be shown. The interference effects of the nozzle jet are small, and for the purpose of the discussion they have been neglected.

For the blades-off configuration the lift coefficient at 12^0 angle-of-attack is about 1.2. By installing the propeller, the overall lift coefficient (i.e. the lift generated by the wing/nacelle/propeller combination) increases to about 1.9 at the same oangle of attack, as can be observed in figure 13 by the increase in overall lift C_{Lwnp} of 0.7. Figure 13 also shows that the lift interference changes of sign at negative angles-of-attack.

Due to the mutual interference and the effect of angle-of-attack on the propeller forces, both the wing/nacelle and the propeller will contribute to the lift increase. As can be seen in figure 14 the larger part of the lift increase is generated by the propeller. At a thrust coefficient of 2.5 and overall lift coefficient C_{Lwnp} of 1.0 the propeller generates about 18% of the lift. The influence of the propeller is significant and one should be careful not to attribute this propeller lift contribution to the lift increase generated by the wing/nacelle combination.

The extra lift in the propeller-on condition as shown above occurs as a result of mutual interferences between the propeller and the airframe. By using the rotating shaft balance, the lift of the propeller can be measured seperatly. The propeller lift curve is shown in figure 15 as well as the relative importance of the normal and axial force components of the propeller shaft force. The contribution of the axial thrust component is somewhat larger than the normal force component. When installed in front of the wing, the propeller will experience different inflow angles compared to the isolated case. In figure 16 the increase in lift of the installed propeller relative to the isolated propeller is visible at different angle-of-attack, the increased upwash in front of the wing results in a larger propeller lift.

Drag

As discussed previously the use of the RSB in combination with an external balance permits a direct analysis of the drag of the wing/nacelle combination. For the purpose of analysis it is useful to make a comparison of the following lift versus drag curves :

- the blades-off lift-drag curve
  (using C_{Lw0} vs. C_{Dwn0}),
- the blades-on overall lift-drag curve
  (using C_{Lwnp} vs. C_{Dwnp}),
- the blades-on wing/nacelle lift-drag curve
  (using C_{Lwn} vs. C_{Dwnp}).

From the comparison in figure 17 it is observed that the favourable inboard-up rotation of the propeller and the lift contribution of the propeller effectively lower the drag, ΔC_{Dwnp} , when compared on basis of the same lift coefficient. For lower lift coefficients the reduction is smaller.

As shown in figure 17 ΔC_{Dwn} is nearly constant up until a lift coefficient of about 0.7 after which the drag reduces slightly to about 100 counts. Apparently the increase of the friction drag on the immersed parts of the wing is offset by the swirl recovery. The swirl recovery is created by the beneficial forward rotation of the large lift vector at the inboard part of the wing which is larger than the adverse rearward rotation of the shorter vector at the outboard parts [7].

The large drag reductions shown in figure 17 are mainly attributed to the influence of a lower angle-of-attack in the blades-on condition. To retain the same overall lift C_{Lwnp}, a lower angle-of-attack is needed than for the blades-off configuration because the propeller contributes a significant part to the overall lift. For the tested configuration this effect on drag is larger than the reduction of the drag of the wing/nacelle due to the slipstream effects (ΔC_{Dwn}) as observed from the comparison of the blades-on and blades-off conditions.

Conclusion

The value of experimental investigations of propeller slipstream effects by means of windtunnel test can be considerably enhanced by using a combination of an external balance and a rotating shaft balance for the measurement of the forces and moments. The bookkeeping of the results of both balances provides detailed information about the interference effects between the propeller and the airframe. In addition, the rotating shaft balance data, such as the thrust coefficient, are available on-line during the measurements. This enables a direct control of the thrust coefficient setting during the test.

By using the pressure measuments, the pressure distribution on the wing, especially on the area immersed in the propeller slipstream, can be studied. Inboard of the nacelle the increased local angle-of-attack results in an increased lift. Contrary to the outboard parts where the negative angles-of-attack reduce the lift. These effects are enlarged by the increased dynamic pressure in the slipstream.

In the near future the results of the measurements will be analysed in more detail by the partners in this joint research. The results will help to obtain improved knowledge on interference effects and will provide a valuable database for the validation of computational codes. Further out in the future follow-on measurements

are planned, aimed at providing additional information such as on interference effects with larger flap deflections and flow field data behind the propeller disk.

Acknowledgment

The authors wish to thank the partners and the colleagues for their support in the JR-01 test campaign in the Indonesian Low Speed Wind tunnel. The large efforts contributed by all parties involved, i.e. IPTN, Fokker, LAGG, NLR, ITB and TU-Delft, to the preparation and execution of the test, are greatly appreciated. The authors also would like to express their appreciation for the valuable input and contributions to this paper provided by partners.

REFERENCES

[1] L.G.M. Custers, Experience with rotating shaft balances for measurements of total propeller force and moment, Indonesian Aircraft Propulsion Symposium 1994, February 1994.

[2] L.G.M. Custers, A.H.W. Hoeijmakers, A.E. Harris, Rotating shaft balance for measurements of total propeller force and moment, 15th International Congress on Instrumentation Aerospace Simulation Facilities, June 1993

[3] G. Fratello, D. Favier, C. Maresca, Experimental and numerical study of the propeller/fixed wing interaction, Journal of Aircraft, June 1991.

[4] H. Muhammad, Identification of turboprop thrust from flight test data, PhD-Thesis, Technical University of Delft, December 1995.

[5] J.D. Price, M.H. Aston, I.F. Burns, Propfan integration on an advanced wing, International forum on Turbine Powered Simulation at DNW, May 1995

[6] G.J. Schipholt, et all, Investigation of methods for modelling propeller-induced flow fields, AIAA 93-0874, January 1993.

[7] L.L.M. Veldhuis, D.W.E. Rentema, Quantative wake surveys behind a tractor propeller-wing configuration, AIAA 95-3908, September 1995

[8] David Witkowski, Alex K.H. Lee, John P. Sullivan, Aerodynamic interaction between propellers and wings, AIAA 88-0665.

[9] Ronald C. Smith and Alan D. Levin, Propfan installation aerodynamics of a supercritical swept wing transport configuration, AIAA 81-1563, July 1981

[10] A.S. Aljabri and A.C. Hughes, Wind tunnel investigation of propeller slipstream interaction with nacelle/wing/flap combinations, AGARD Symposium on Aerodynamics and Acoustics of Propeller, October 1984.

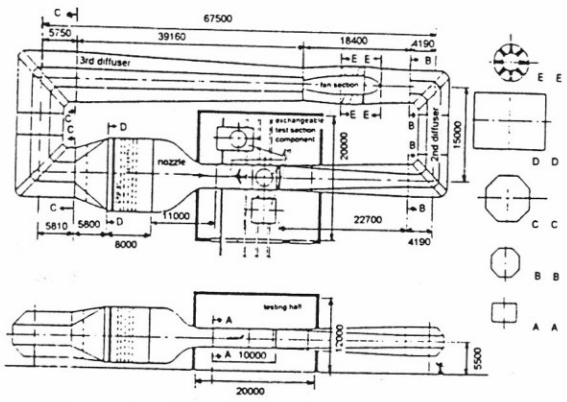

Figure 1. Lay out of Indonesian Low Speed Wind Tunnel

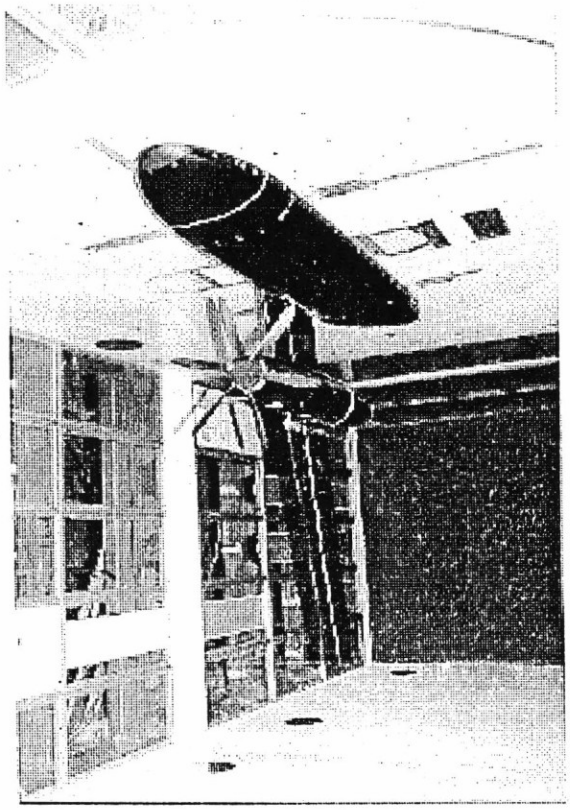

Figure 2. The model installed in the test section

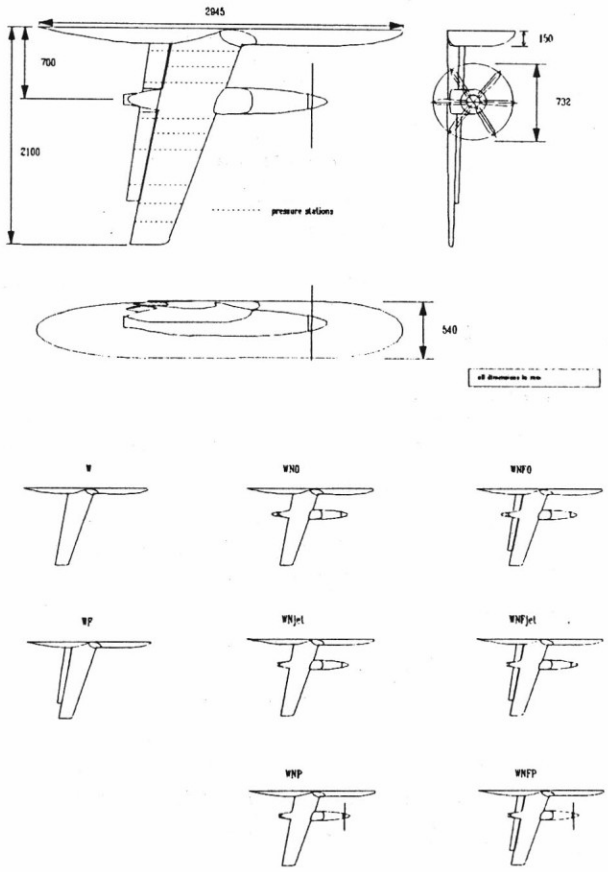

Figure 3. General arrangement of the half model and the basic configurations

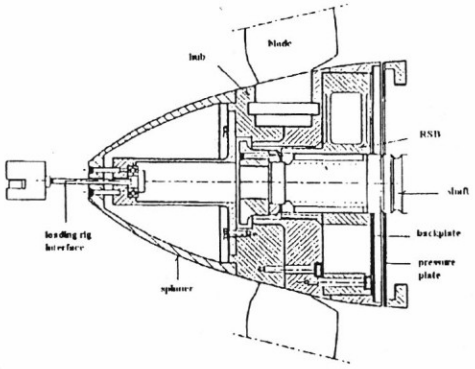

Figure 4. Lay out of the hub

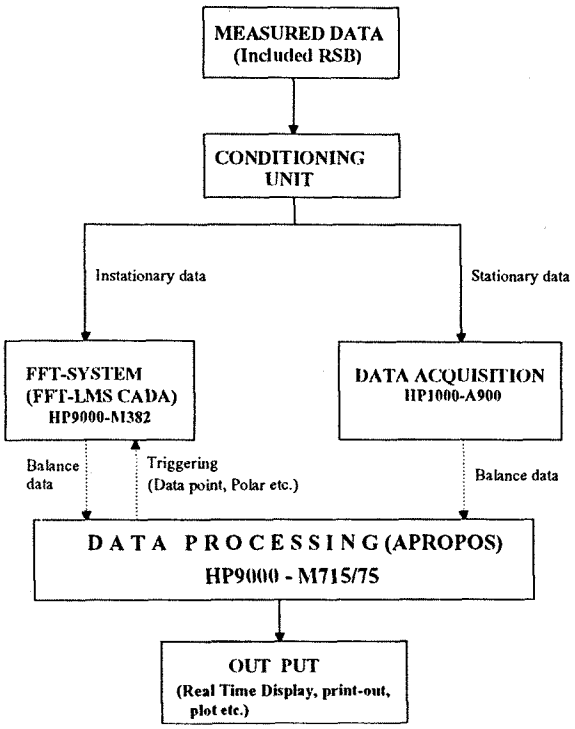

Figure 5. Scheme of the Data Acquisition and Data Processing

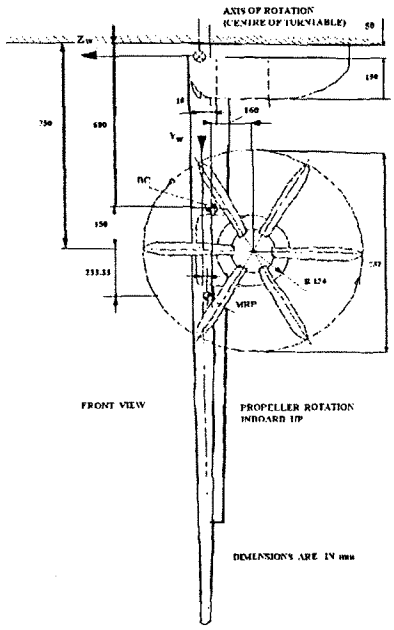

Figure 6. The position of Moment Reference Point

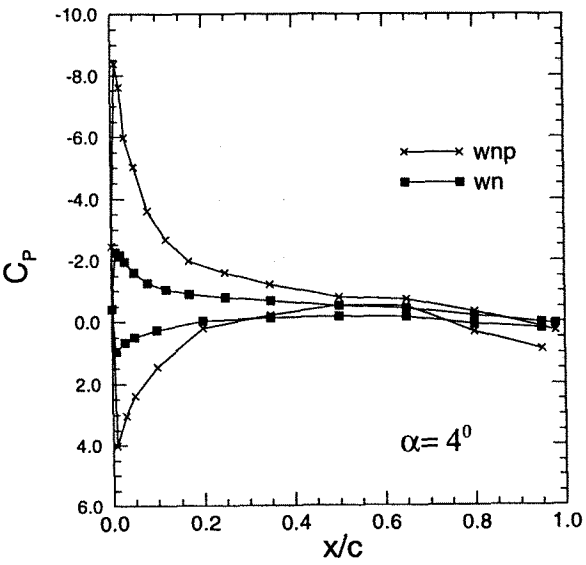

Figure 7. Inboard (section 3)Cp distribution of WNP and WN configuration

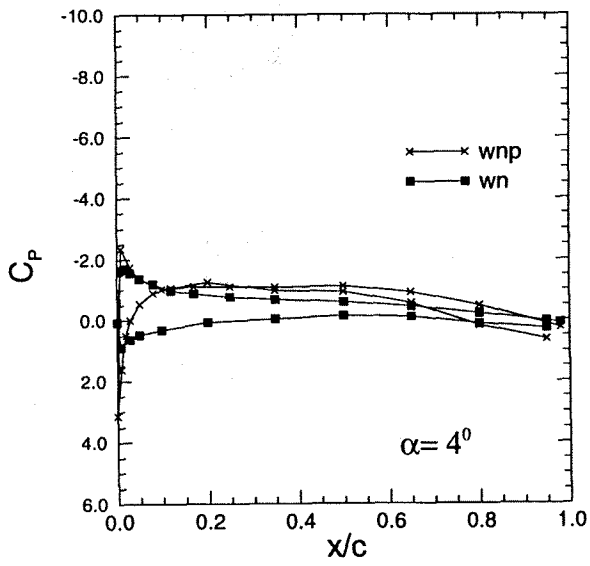

Figure 8. Outboard (section 4) Cp distribution of WNP and WN configuration

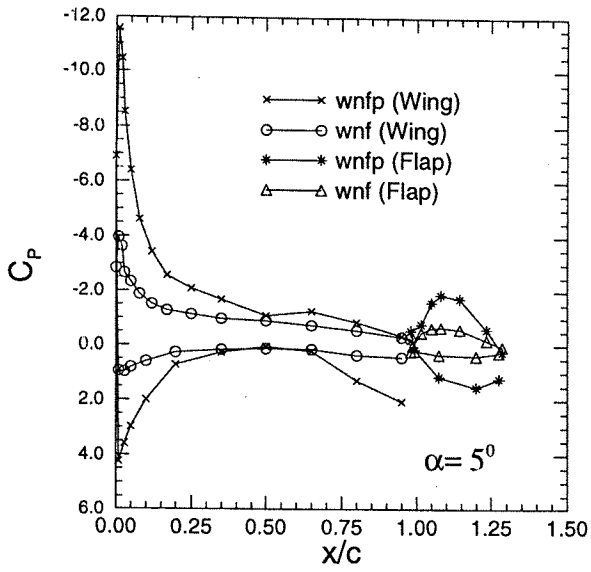

Figure 9. Inboard (section 3) Cp distribution of WNFP and WNF configurations

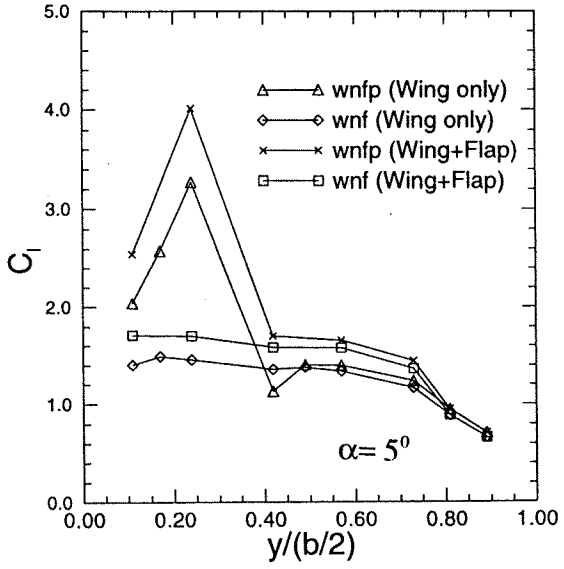

Figure 11. Spanwise lift distribution of WNFP and WNF configurations

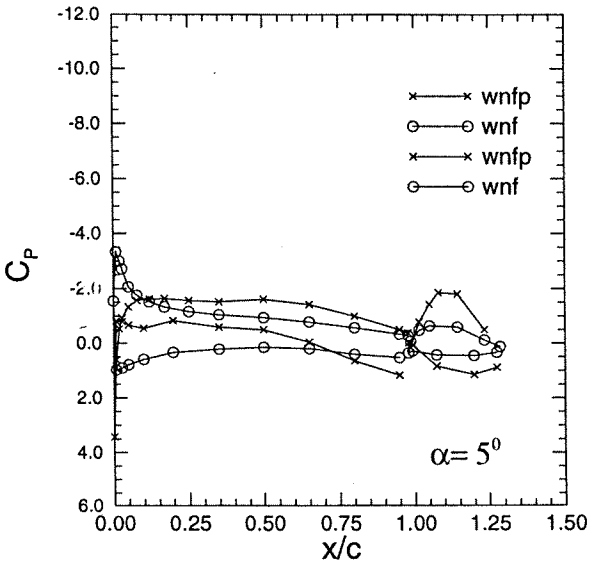

Figure 10. Outboard (section 4) Cp distribution of WNFP and WNF configurations

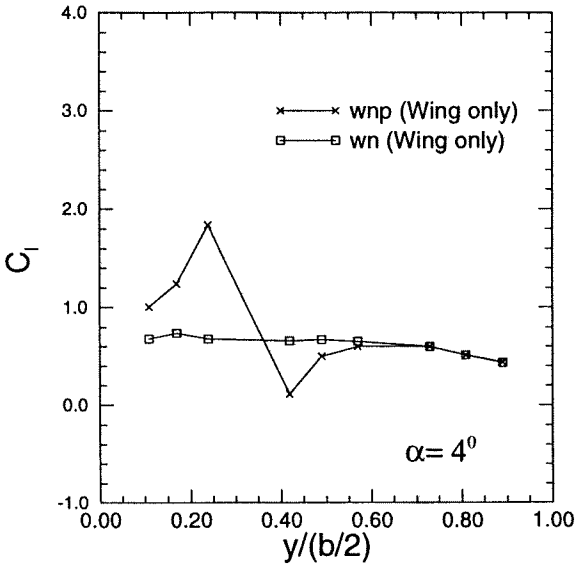

Figure 12. Spanwise lift distribution of WNP and WN configurations

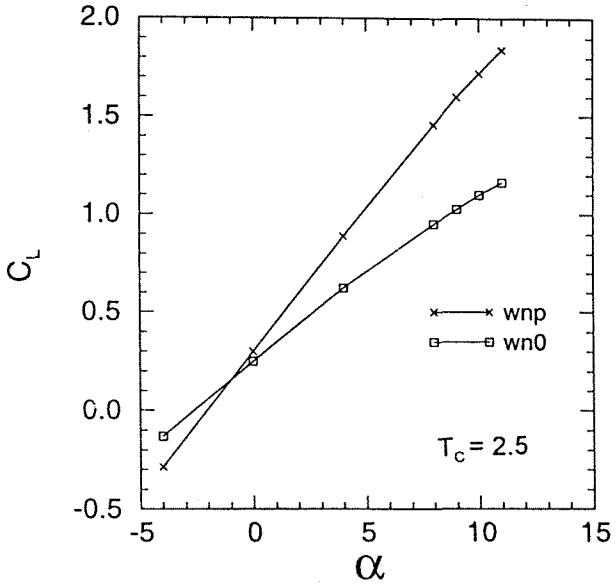

Figure 13. C_L - α graph of WNP configuration

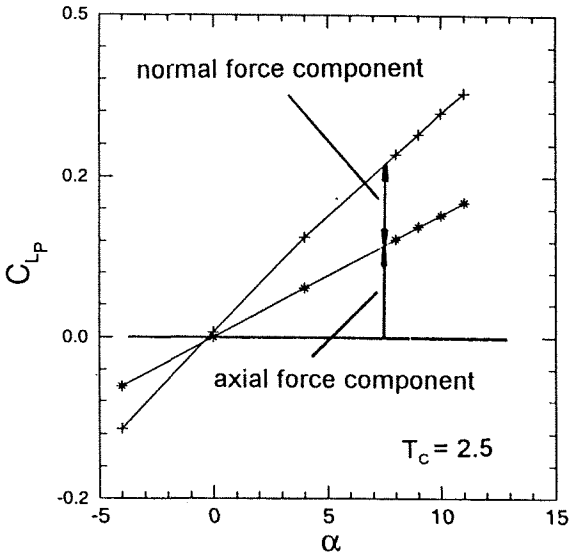

Figure 15. Contributions of the axial thrust component and the normal force component to the propeller lift

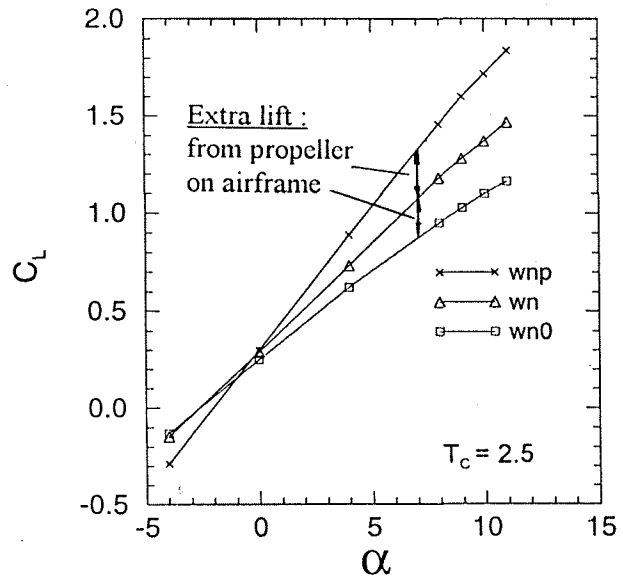

Figure 14. C_L breakdown of WNP configuration

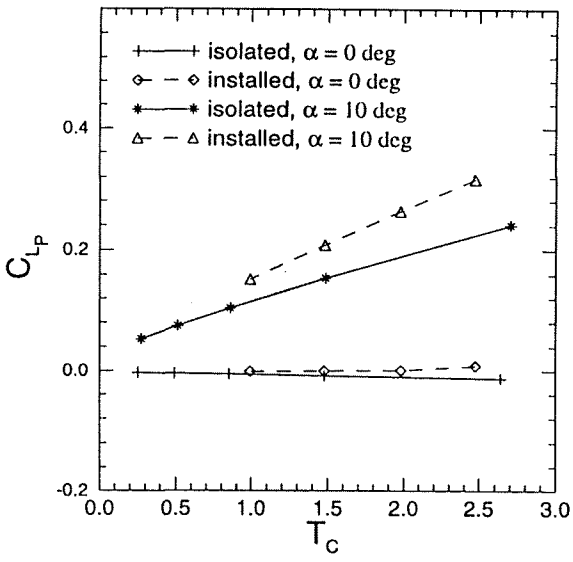

Figure 16. Propeller lift of the installed and isolated propeller

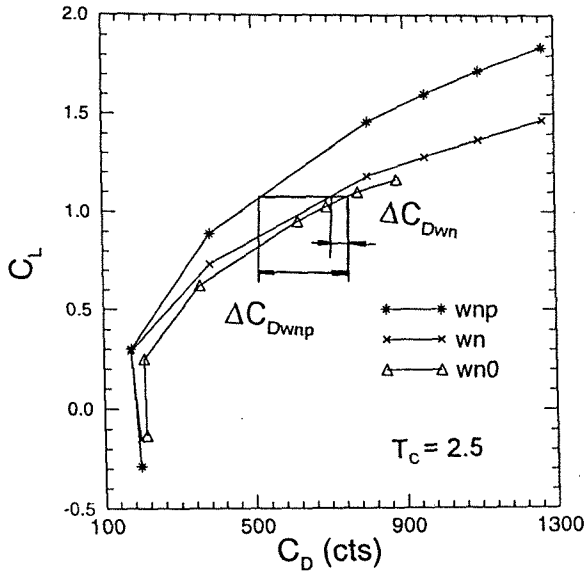

Figure 17. Comparison and breakdown of the lift-drag curve